PROCEEDINGS, 50th Workshop on Geothermal Reservoir Engineering
Stanford University, Stanford, California, February 10-12, 2025
SGP-TR-229

Preliminary Depth to Basement Modeling at Salton Sea, California

Jacob Anderson[1], Jonathan Glen[1], William Schermerhorn[1], Tait Earney[1], Benjamin Morbeck[1]

[1]U.S. Geological Survey, 350 N. Akron Rd., Moffett Field, CA 94035, USA

jeanderson@usgs.gov

Keywords: Salton Sea, Imperial Valley, southern California, San Andreas Fault, Imperial Fault, Salton Sea geothermal system, geophysics, geothermal systems, magmatic systems, tectonic systems, mineral resources, gravity, modeling, lithium

ABSTRACT

The San Andreas Fault – Imperial Fault (SAF-IF) transtensional step-over zone along the southern margin of the Salton Sea hosts substantial geothermal production and lithium brine resources. Recent volcanism at the Salton Buttes and active seismicity along the SAF-IF fault system highlight active tectonic and magmatic processes that pose natural hazards and may impact energy and mineral production. Characterizing the subsurface architecture and extent of concealed alteration associated with this tectono-magmatic system enhances understanding of these active processes, associated hazards, and resources.

We have compiled a gravity database, consisting of new and re-processed existing data, from which we have constructed a new isostatic residual gravity anomaly map of the Salton trough. We have used this new gravity dataset together with a compilation of publicly available borehole data to develop new depth to basement inversion models for the region. These depth to basement models help to constrain basin geometries, inform alteration mapping, and reveal variations in basement rocks. Due to the concealed nature of the complex tectonic framework at the Salton trough, it is necessary to utilize geophysical methods for subsurface characterization. These new depth to basement models are a first step toward constructing 2D and 3D geophysical and geologic models of the Imperial Valley and Salton Sea geothermal area. This analysis complements other geophysical initiatives, including magnetotelluric (MT) modeling (Tokmakoff et al., 2024), magnetic mapping (Glen and Earney, 2023, 2024) and potential field modeling, and seismic studies focused on hazard and resource investigations in the Imperial Valley.

1. INTRODUCTION

The Salton trough is an active continental rift representing the northern-most expression of the Gulf of California rift system (Elders et al., 1972). Cyclical episodes of lake formation and evaporation have increased the salinity of subsurface aquifers, which, paired with elevated heat flow and magmatic intrusions have developed a metalliferous brine (McKibben et al., 1988). The high heat flow (Lachenbruch et al., 1985) and extensive brine resource have created a unique opportunity for co-production of geothermal energy and lithium extraction at the Salton Sea Geothermal Field (SSGF, Figure 1).

Because these resources are concealed within young sedimentary basin fill, utilizing geophysical methods can enhance understanding of the complex subsurface architecture and rock property distribution present across the SSGF and greater Salton trough region. The San Andreas Fault – Imperial Fault (SAF-IF) transtensional step-over zone contributes structural complexity across the entire trough, imposing major tectonic and magmatic controls over the SSGF. The tectonic and volcanic state of the Salton trough is relatively young. Brothers et al. (2009) estimate the age of the SAF-IF step-over zone to be no older than 0.5 Ma and Schmitt and Hulen (2008) suggest the Salton Buttes and buried intrusive units span at least 0.4 Ma.

Elevated heat flow (Lachenbruch et al., 1985) and volcanic activity at and around the SSGF have produced extensive metamorphism at depth within the sediments (Muffler and White, 1969). McKibben et al. (1988) observes that the combination of a high heat flux from rift-related magmatism and an enriched metalliferous brine produces pervasive metamorphism of shallow sediments, accompanied by secondary mineralization of calcite, sulfides, carbonates, and hematite. These processes increase the bulk density of sediments. This densification of sediments, particularly beneath the SSGF, has complicated seismic (Fuis and Kohler, 1984; Han et al., 2016) and gravity interpretations (Biehler, 1964). Constructing a geophysical and structural model of this system requires additional efforts to understand the extent of metamorphism and its contribution toward observed geophysical anomalies. We use existing and new gravity data across the Salton trough (Figure 2) and localized at the SSGF (Figure 3) to model the depth to basement across this region. Modeling the depth to basement integrates information from gravity, mapped geology, and subsurface contacts from borehole logs, to provide approximations of basin geometry. Primarily, this technique is sensitive to changes in bulk density which provides an opportunity to compare with seismic results from previous studies, which depend on similar physical properties.

Araya and O'Sullivan (2022 and references therein) observe the impermeable clay cap present beneath the SSGF to correspond with the interface between shallowly conductive and deeply convective heat transfer. In their 3D conceptual and natural-state models, Araya and O'Sullivan (2022) define the clay cap using conductivity data from Nichols (2009) as 0.2 – 0.4 Ohm-M. However, several factors including temperature, salinity, and porosity can influence resistivity at depth (Nichols, 2009; Araya and O'Sullivan, 2022). Despite this complexity, the highest concentration of dissolved metals is found within the hypersaline brines (McKibben et al., 1987; Araya and O'Sullivan, 2022). We therefore approximate the clay cap to represent (1) the boundary of the productive geothermal reservoir where high metal concentrations (specifically lithium) are present, and (2) the minimum depth to metamorphosed sediments.

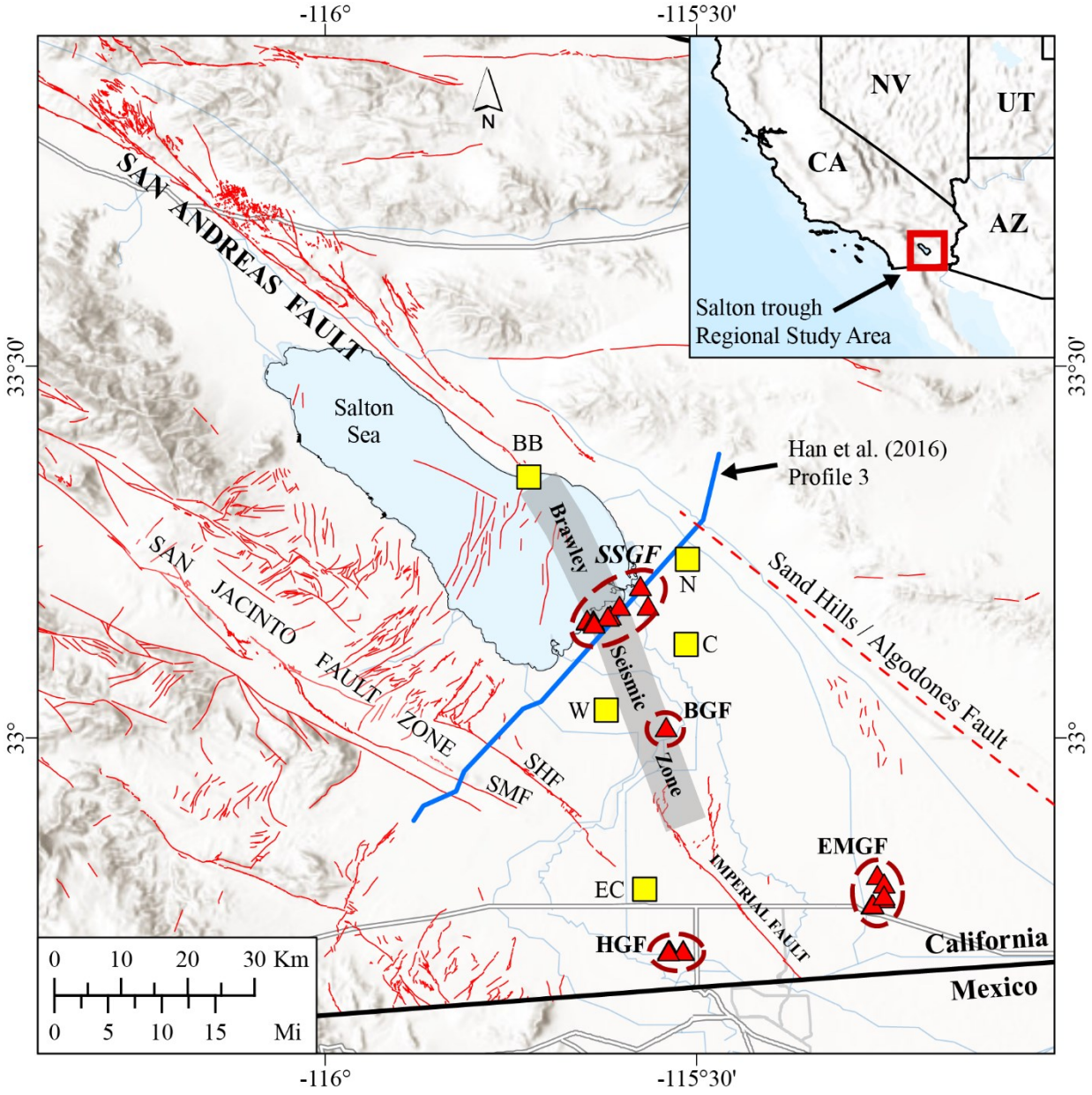

Figure 1: The Salton trough study area with elevation hillshade (Esri, 2024). Top right inset shows the regional study area location. Red lines are Quaternary faults from U.S. Geological Survey (2020). Blue line is seismic profile 3 from Han et al. (2016). The red dashed ellipses surround red triangles which are operating geothermal power plants from the National Renewable Energy Laboratory (2014). The dashed red line is the inferred trace of the Sand Hills / Algodones Fault following figure 1 of Han et al. (2016). SSGF, Salton Sea Geothermal Field; BGF, Brawley Geothermal Field; HGF, Heber Geothermal Field; EMGF; East Mesa Geothermal Field; SHF, Superstition Hills Fault; SMF, Superstition Mountain Fault; BB, Bombay Beach; N, Niland; C, Calipatria; W, Westmorland; EC, El Centro.

2. METHODS

We modeled the depth to basement following the method of Jachens and Moring (1990) and Jachens et al. (1996). We first generalized geology from the California State Geologic Map (Jennings et al., 2010) across the entire region of interest into three categories that reflect density groupings. These categories are loosely defined as (1) Cenozoic sediments, (2) Cenozoic volcanic rocks, and (3) Pre-Cenozoic crystalline basement. Depth to basement procedures were developed within the context of characterizing basin cover thickness and basement density variations in the Basin and Range Province, primarily Nevada (Jachens and Moring, 1990; Saltus and Jachens, 1995). This routine assumes a significant contrast in rock density between Cenozoic sediments (2.02 – 2.42 g/cm^3) and Pre-Cenozoic crystalline basement rocks (2.67 g/cm^3). Given the inherent density variability of volcanic rocks, we have made two separate calculations: (1) where volcanics are considered to have densities equal to sediments, and (2) where volcanic density is equal to crystalline basement.

The isostatic residual gravity anomaly field was then calculated for the study area using standard reduction methods after Blakely (1995). The calculation included 1,644 new gravity stations collected during 2023 and 2024 field campaigns and supplement the over 15,000 existing regional gravity stations in the area (Figure 2; Hildenbrand et al., 2002 [PACES]; PACES database was made available from University of Texas, El Paso on 5/29/2018 [Ben Drenth, U.S. Geological Survey, written comm., March 2021]). A density-depth function is needed to convert gravity anomalies reflecting the distribution of low-density basin fill to basin thicknesses. This density-depth function factors compaction and lithification processes into the calculation, following Jachens and Moring (1990) and Jachens et al. (1996): 2.02 g/cm^3 from 0-200 m depth; 2.12 g/cm^3 from 200-600 m depth; 2.32 g/cm^3 from 600-1200 m depth; and 2.42 g/cm^3 at depths greater than 1200 m.

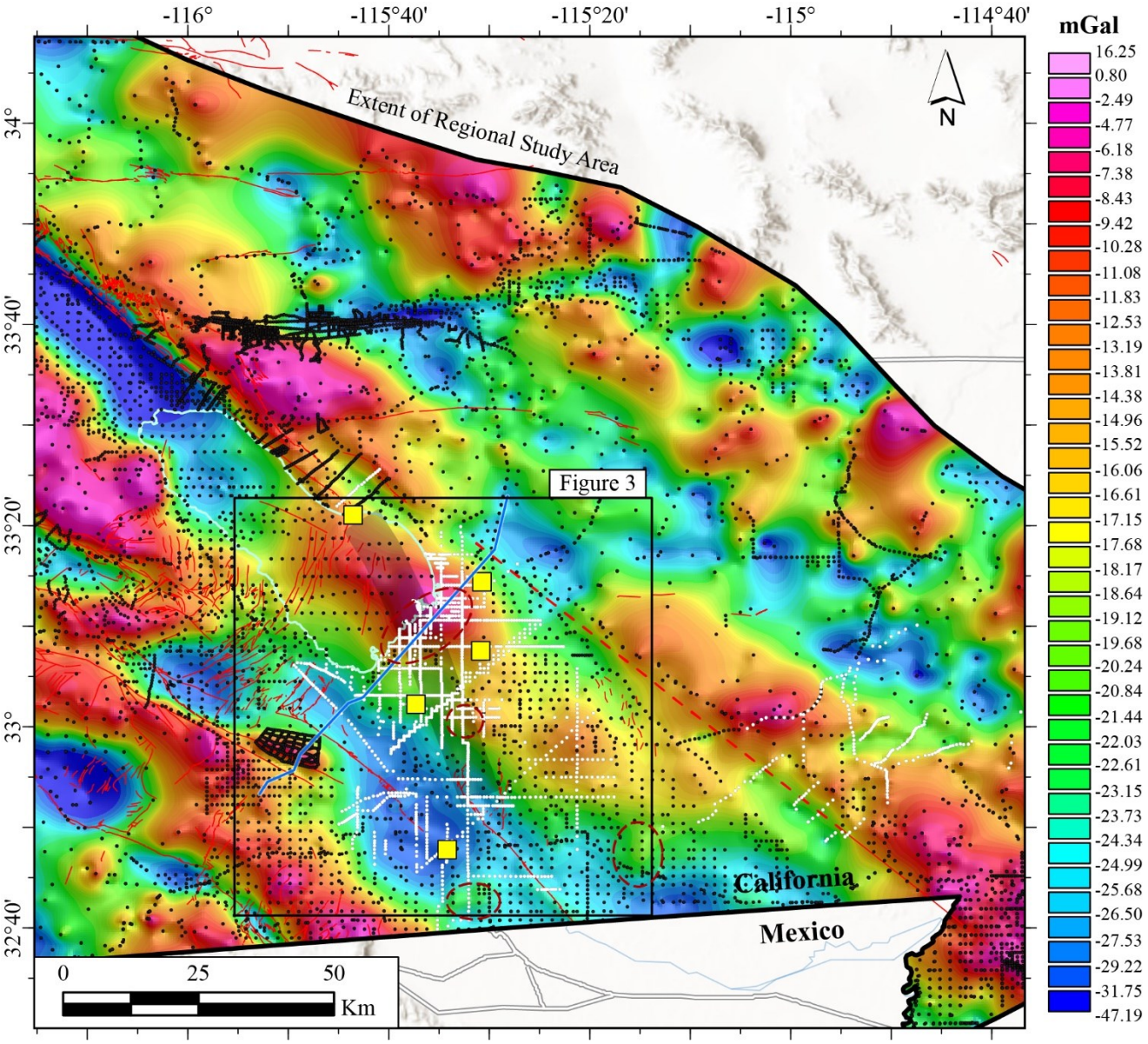

Figure 2: Isostatic residual gravity anomaly map across the Salton trough with elevation hillshade (Esri, 2024) beneath. Black circles are existing stations and white circles are new stations. Gravity stations that are closely spaced may resemble lines. Red dashed ellipses and yellow squares correspond to geothermal power plants and towns (respectively) identified in figure 1. Red lines are Quaternary faults from U.S. Geological Survey (2020). The dashed red line is the inferred trace of the Sand Hills / Algodones Fault following figure 1 of Han et al. (2016). The dark blue line is seismic profile 3 of Han et al. (2016). The light teal line is the outline of the Salton Sea.

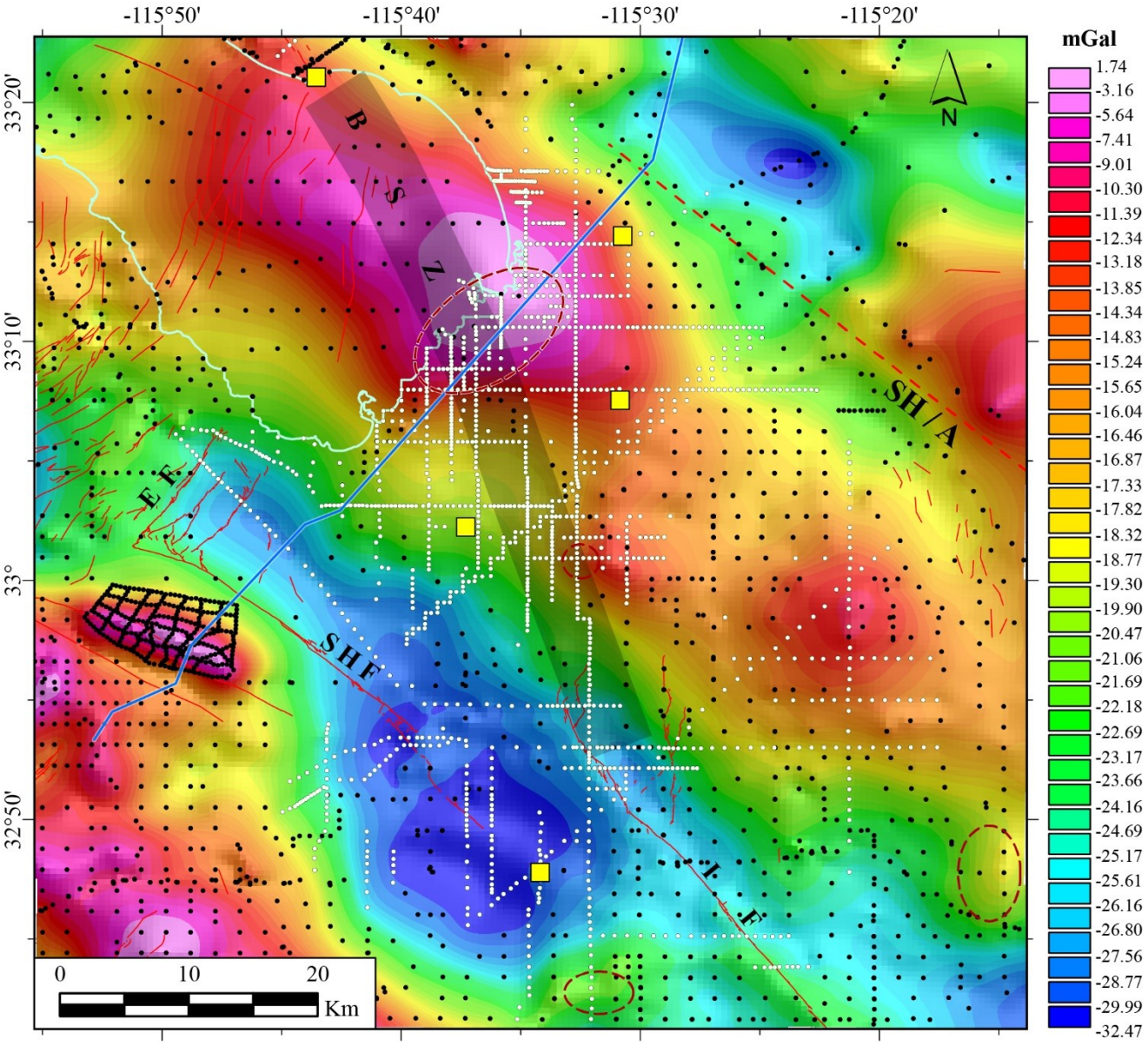

Figure 3: Isostatic residual gravity anomaly across Imperial Valley and the SSGF. Black circles are existing stations and white circles are new stations. Gravity stations that are closely spaced may resemble lines. Yellow squares correspond to towns identified in figure 1. Red dashed ellipses outline geothermal power plants from figure 1. Red lines are Quaternary faults from U.S. Geological Survey (2020). The dashed red line is the inferred trace of the Sand Hills / Algodones Fault following figure 1 of Han et al. (2016). The blue line is seismic profile 3 of Han et al. (2016). BSZ, Brawley Seismic Zone; IF, Imperial Fault; SHF, Superstition Hills Fault; SH / A, Sand Hills / Algodones Fault; EF, Elmore Ranch Fault.

An iterative procedure is used to progressively converge toward an acceptable depth to basement solution wherein further iterations return a result with no substantial change from the previous run. The procedure has two main steps: first, separating the gridded isostatic residual gravity anomaly into two components reflecting the gravity effect of (1) low-density basin fill, and (2) the distribution of underlying basement rocks. The second step involves converting the gravity effect from low-density basin fill into a grid of estimated basin thickness. The first iteration computes a grid of the "basement gravity anomaly" by interpolating the isostatic residual anomaly from stations that are only located on basement outcrops across the entire study area and across intervening basins. Then, the difference between the basement gravity anomaly grid and the observed isostatic residual gravity anomaly grid is computed, representing the effect from low-density basin fill: the "basin gravity anomaly". Finally, the basin gravity anomaly grid is converted to a grid of sediment thickness, the "basin depth", using density contrasts between basement rocks and sediments with a density-depth function as described above. The succeeding iterations use the estimated basin gravity anomaly to calculate the effect from nearby low-density basin fill on gravity stations located on basement. This effect is removed from the observed anomalies and the process is repeated. Where borehole logs are available, the depths of basement rock intersection are incorporated as constraints for the modeling process.

Publicly available borehole data from the California Geologic Energy Management (CalGEM) Division's online database (www.conservation.ca.gov/calgem/Pages/WellFinder.aspx) are used to determine depth to basement at localized sites within the Salton trough. For the depth to basement models where the density of volcanic deposits is considered equal to basement rocks, we generally classified volcanic deposits greater than 50 feet thick as basement. In the case where we considered volcanic rocks as having densities equivalent to sediments, we only used well constraints when crystalline basement lithologies were encountered. The resulting basement picks provide valuable constraints to the basement inversion.

A major complication in the Salton trough is the lack of a sharp contrast between cover deposits and crystalline basement due to metamorphosed sediments at depth (Muffler and White, 1969). These metamorphosed rocks gradually grade towards densities equivalent to that of basement, complicating seismic interpretations (Han et al., 2016) that typically rely on unambiguous rock property contrasts. To characterize the top to this altered sediment package, we define these altered rocks as basement. We pin the basement surface in the area of the SSGF to the top of the clay cap as defined by Araya and O'Sullivan (2022).

3. RESULTS

We present four models of depth to basement from this gravity analysis for each geology category: (1) where volcanic rocks are considered crystalline basement (Figures 4A-4D), and (2) where volcanic rocks are equal to sediments (Figures 4E-4H). The first models (Figures 4A and 4E) are unconstrained, reflecting the approximation of basin depths based only on mapped geology and the isostatic residual gravity anomaly. The second models (Figures 4B and 4F) are constrained at depth by the clay cap, following the method of Araya and O'Sullivan (2022) for wells within the SSGF. The third models (Figures 4C and 4G) are constrained with borehole picks based on lithology. Figure 4C uses picks where either volcanic units or crystalline basement is intersected. Figure 4G uses picks where only crystalline basement is intersected. The fourth models (Figures 4D and 4H) are hybrid, using the clay cap picks and borehole lithology picks only where crystalline basement is intersected (for both geologic categories).

The "unconstrained" depth to basement model in figure 4A shows an elevated basement surface near the SSGF approximately 10 x 10 kilometers in size. This model indicates a shallowing of the basement along a NW-SE axis. There is very little variation of basin depth along a SE trend from Bombay Beach (BB) to Niland (N), eventually broadening out toward the BSZ south of Calipatria (C). The relatively flat basement surface in this region is interrupted by two shallow platforms, one coincident with the Brawley Geothermal Field (BGF) and one about 10-20 kilometers NW from the East Mesa Geothermal Field (EMGF). The deepest basin occurs within the left step-over between the Superstition Hills Fault (SHF) and the Imperial Fault (IF), coincident with a major basin modeled by Persaud et al. (2016). Between Westmorland (W) and Niland, the depth to basement resembles a dome-like shape, reaching shallowest depths at the SSGF.

The depth to basement model constrained by clay alteration in figure 4B is similar to the unconstrained model (Figure 4A), with two notable differences. First, using clay alteration constraints, a basin adjacent to Niland is modeled approximately 1 km deeper than the unconstrained model. Second, the zone of very shallow basin depth (0 – 100 m) is more tightly constrained along a NNE-SSW trend near the SSGF and slightly deeper basin depths (100-500 m) exhibit a more pronounced NE-SW trend parallel to the southern shore of the Salton Sea. The dome-shape characteristic across a NE trend from Westmorland through Niland is present here, though with a steeper gradient near Niland compared to the unconstrained model (Figure 5).

The depth to basement model constrained by geothermal and oil and gas well picks (Figure 4C) suggests substantial differences compared to the clay alteration and unconstrained models (Figures 4A and 4B, respectively). The basin is deepest from Niland along a SE trend, reaching depths in excess of 6.5 km. Basin depths across the study area are approximately 500 m – 1 km deeper than in the unconstrained and alteration models. The NW-SE elongate basin modeled in the unconstrained and clay alteration models at the step-over between the SHF and IF is absent in this model whereas a smaller, WNW-ESE oriented basin near Westmorland is modeled (Figure 4C).

The hybrid model shown in figure 4D captures the shallow basin depths at the SSGF present in the clay alteration model (4B) while deepening the basin next to Niland, though not quite reaching the depths modeled with constraints from borehole picks (Figure 4C). The four boreholes located southeast from Calipatria are not used as constraints for this model which has the effect of shallowing basin depths across the entire eastern trough. Notably, this hybrid model reproduces the deep basin between the SHF and IF present in the unconstrained and clay alteration models (Figures 4A and 4B).

Modeling the depth to basement where the density of volcanic units is equal to sediments produces similar results to those where volcanics are considered equal to basement with some substantial differences. The unconstrained model (Figure 4E) matches its counterpart (Figure 4A) except along the eastern trough where basement surfaces are elevated. In addition, the 0 – 100 m thickness zone at the SSGF is more extensive toward the NE. The clay alteration model (Figure 4F) again closely matches the model where volcanics are equal to basement (Figure 4B) except at the SSGF where the model estimates the basin to be deeper. The model constrained by borehole picks (Figure 4G) is substantially different to that where volcanics are equal to basement (4C). This model (Figure 4G) used 17 borehole picks where only intersections of basement lithologies were encountered (typically granodiorites), compared to figure 4C where 33 borehole picks were used to constrain the basin depths from basement and volcanic intersections. The hybrid model (Figure 4H) closely matches its counterpart (Figure 4D), with the only notable difference arising at the SSGF, where basin thicknesses are deeper.

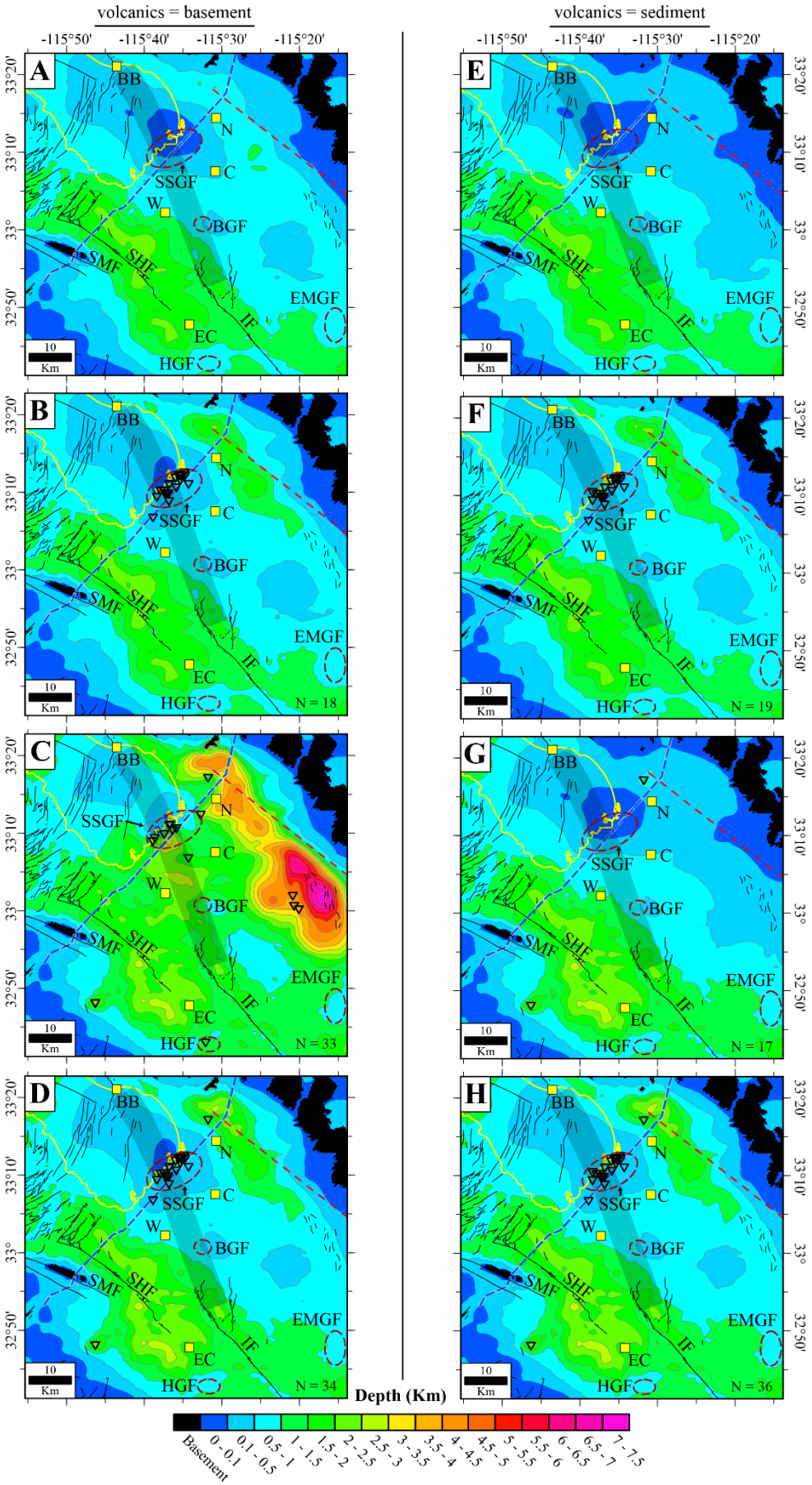
volcanics = basement
volcanics = sediment
-115°50'
-115°40'
-115°30'
-115°20'
33°20'
33°10'
33°
32°50'
A
B
C
D
E
F
G
H
BB
N
C
W
SSGF
BGF
SMF
SHF
IF
EMGF
EC
HGF
10
Km
N = 18
N = 33
N = 34
N = 19
N = 17
N = 36
Depth (Km)
Basement
0 - 0.1
0.1 - 0.5
0.5 - 1
1 - 1.5
1.5 - 2
2 - 2.5
2.5 - 3
3 - 3.5
3.5 - 4
4 - 4.5
4.5 - 5
5 - 5.5
5.5 - 6
6 - 6.5
6.5 - 7
7 - 7.5

Figure 4: Depth to basement models. A-D: volcanic density considered equal to crystalline basement, E-H: volcanic density considered equal to sediments. A, depth to basement with no well constraints; B, depth to basement where the depth to clay alteration, following Araya and O'Sullivan (2022), is considered basement; C, depth to basement with geothermal and oil and gas borehole constraints; D, a hybrid depth to basement model where we use the clay alteration picks following Araya and O'Sullivan (2022) and borehole picks that encounter only crystalline basement lithologies as constraints for the model. E-H: The same kinds of depth to basement models as A-D in sequence for side-by-side comparison. The number of wells used to constrain each model are given in the bottom right corner. Boreholes used to constrain the model are shown as inverted triangles. Yellow squares and red dashed ellipses are features identified in figure 1. The blue dashed line is seismic profile 3 of Han et al. (2016). Black lines are Quaternary Faults from U.S. Geological Survey (2020). The dashed red line is the inferred trace of the Sand Hills / Algodones Fault following figure 1 of Han et al. (2016). The broad grey zone extending from the Imperial Fault to the San Andreas Fault is the Brawley Seismic Zone. IF, Imperial Fault; SHF, Superstition Hills Fault; SMF, Superstition Mountain Fault; BB, Bombay Beach; N, Niland; C, Calipatria; W, Westmorland; EC, El Centro; SSGF, Salton Sea Geothermal Field; BGF, Brawley Geothermal Field; HGF, Heber Geothermal Field; EMGF, East Mesa Geothermal Field.

4. DISCUSSION

The depth to basement models share broad trends across the Salton trough while indicating additional complexity coincident with and east from the SSGF. The SSGF is characterized by an elevated basement surface for all models between 0 and 500 m thickness. This trend is consistent with observations of metamorphosed sediments at depth (Muffler et al., 1969), as well as high seismic velocities below the SSGF (Persaud et al., 2016; Han et al., 2016) arising from high density in the subsurface resulting from metamorphism. In addition, all models agree with findings from Persaud et al. (2016) delineating a basin between the Superstition Hills and Imperial Faults. Our results indicate the basin is considerably shallower than suggested by Persaud et al. (2016), but this likely reflects the differences between defining "basement". As shown in figure 5, the 5.65 km/s surface was taken to represent the basement contact by Persaud et al. (2016) whereas our results indicate basement rocks corresponding to the 3.7 km/s contour at the deepest point (approximately at 19-20 line-km on figure 5).

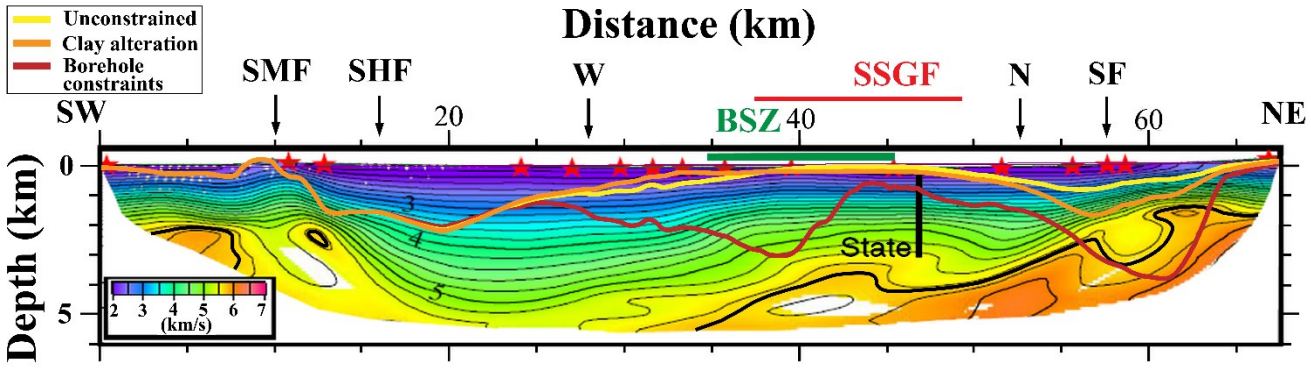

Figure 5: Depth to basement surfaces along seismic line 3 of Han et al. (2016) showing Vp in km/s. Figure is modified from figure 9 of Han et al. (2016). The yellow line is from the unconstrained model (Figure 4A), the orange line is constrained by clay alteration (Figure 4B), and the red line is constrained with geothermal and oil and gas borehole picks (Figure 4C). The bold black line is approximate location of 5.65 km/s surface defined as basement in Persaud et al. (2016). Red stars are seismic shot locations. SSGF, Salton Sea Geothermal Field; BSZ, Brawley Seismic Zone; SMF, Superstition Mountain Fault; SHF, Superstition Hills Fault; SF, Sand Hills Fault; W, Westmorland; N, Niland. Vertical black line is State 2-14 well, included from figure 9 of Han et al. (2016).

If this basin, observed by Persaud et al. (2016) and this work, do represent an older extensional inherited structure, it is possible that sediments at depth have been metamorphosed similarly to those below the SSGF. However, a simpler explanation is possible. The elevation of the basement surface from ~20 line-km to ~55 line-km (Figure 5) forming a dome-like structure could represent a broad zone of subsurface metamorphism due to present activity at and around SSGF. If metamorphism of basin sediments is laterally extensive at depth, the modeled basin depths across the majority of the Salton trough would be anomalously shallow. The differences present between the unconstrained (Figure 4A) and borehole (Figure 4C) models southeast from the SSGF reflect this discrepancy between known basin depths of at least 3-3.5 km and estimated basin depths of less than a kilometer. The gravity anomalies in this region (Figure 3) drive the basin to moderate (<1 km) depths in the unconstrained model, whereas the borehole model produces basins as deep as nearly 7 km. This 7 km deep basin is likely an overestimation resulting from pervasive metamorphism that may be structurally controlled. Regardless, the surface produced in the unconstrained model represents, in all likelihood, the depth to alteration rather than depth to crystalline basement.

The unconstrained and clay alteration depth to basement surfaces are nearly identical, with deviations occurring along the southwest and northeast margins of the SSGF (Figure 5). The depth controls present for the clay alteration model elevate the basement surface on the southwest side, potentially indicating a thicker package of metamorphosed sediments than suggested in the unconstrained model. The most noticeable discrepancy occurs at the northeast end of the profile where the clay alteration model shows a basin nearly 2 km deep, approximately 1 km deeper than in the unconstrained version (Figure 5). This difference indicates that alteration at depth could be less extensive toward the northeast, potentially due to inactivity of hydrothermal circulation or structural control preventing alteration

processes from reaching northeast. Alternatively, tectonic activity localized at the Sand Hills Fault (SF) may explain the model results. Both the depth to basement models and the velocity model from Han et al. (2016) show large deviations at the Sand Hills Fault intersection. A damage zone at depth may be responsible for the velocity embayment and may contribute toward the increased basin depth as bulk density is decreased within the zone, leading to an overestimation of basin depth.

The borehole model in figure 5 defined basement by lithology rather than alteration. However, this basement surface shows substantial undulation between the Brawley Seismic Zone and Sand Hills Fault that, though not present in the unconstrained or alteration model versions, may also be reflecting tectonic control on bulk density (Figure 5). This undulation occurs coincident with the BSZ and SF, where the surface is deepest, and at the SSGF, where the surface is shallowest. A damage zone may be responsible for the deepening of the basin at the BSZ (~38-39 line-km) and SF (~60 line-km) intersections. The adjacent basement high, located directly beneath the SSGF, may reflect alteration and metamorphic processes that locally raise the bulk densities of basin fill.

5. CONCLUSIONS

New preliminary depth to basement models have been constructed at the Salton trough to investigate the extent of metamorphism in the subsurface at and around the Salton Sea Geothermal Field. Four versions of the models presented were considered: (1) an unconstrained model with no subsurface controls imposed, (2) an alteration model where metamorphosed sediments intersected along the southern margin of the Salton Sea are taken to represent basement, (3) where intersections with typical basement lithologies (dense volcanic rocks, dikes, crystalline basement, etc.) are used to control depth estimations, and (4) where alteration at the SSGF and crystalline basement intersections are used to constrain the model. Comparison with previous work from Persaud et al. (2016) finds broad agreement in geometry and locations of basins but differences arise when comparing the magnitude of basin depths. Comparison with seismic tomography from Han et al. (2016) overlain with the basement contact defined in Persaud et al. (2016) in figure 5 clearly show a discrepancy between absolute depth values. However, some important similarities and findings are evident:

1) A concealed basin between the Superstition Hills and Imperial faults is observed, agreeing with findings from Persaud et al. (2016) and mimicking the seismic contours presented by Han et al. (2016).
2) Both the unconstrained and alteration depth to basement models indicate an elevated basement surface between 20 and 55 line-km along seismic profile 3 (Figure 5), potentially indicating the presence of a broad zone of metamorphosed sediments.
3) The undulatory depth to basement surface from the borehole model (Figure 5) is coincident with the Brawley Seismic Zone, the Salton Sea Geothermal Field, and the Sand Hills Fault, suggesting bulk physical properties here reflect a complex interplay between tectonic and magmatic process. Damage zones associated with the BSZ and SF may lower bulk density while alteration and metamorphism at the SSGF elevate bulk density.

The striking difference between basin depths between the unconstrained, clay alteration, and borehole models (Figure 5) are most evident along the eastern margin of the Salton trough, at the SSGF, and south of the SSGF. Geothermal wells in the southeastern trough do not intersect igneous intrusions until reaching depths deeper than 12,000 feet (3,650+ m) (CalGEM Division, 2024), suggesting the basin depths in the unconstrained and clay alteration models are considerably too shallow. Once we incorporate borehole constraints into the model the basin depths increase substantially. However, all models show shallow basement at SSGF extending well into the Salton Sea.

These results highlight the importance and difficulty of defining “basement” in the Salton trough. Different definitions and methods of constraining basement at depth yield major differences between estimations of basin depths across the Salton trough and at the SSGF. To improve depth to basement modeling, additional efforts to digitize geophysical well logs, particularly density logs, are needed to conduct a comprehensive analysis of an appropriate density-depth function for the Salton trough. Lastly, 2D joint modeling across the Salton trough using both gravity and magnetic data could illuminate the favorability of these results and better characterize basin and basement geology.

ACKNOWLEDGEMENTS

We thank Daniel Scheirer and Grant Rea-Downing for their thoughtful reviews that greatly improved this manuscript. This work was funded with support from the U.S. Geological Survey Energy Resources Program. Any use of trade, firm, or product names is for descriptive purposes and does not imply endorsement by the U.S. Government.

REFERENCES

Araya, N. and O’Sullivan, J.: A 3D Conceptual and Natural-State Model of the Salton Sea Geothermal Field, GRC Transactions, 46, (2022), 2123-2155.

Biehler, S., 1964.: A geophysical study of the Salton Trough of southern California (Doctoral dissertation, California Institute of Technology). doi: 10.7907/ZZ33-6E45

Blakely, R.J.: Potential theory in gravity and magnetic applications, Cambridge University Press, (1995).

Brothers, D.S., Driscoll, N.W., Kent, G.M., Harding, A.J., Babcock, J.M. and Baskin, R.L.: Tectonic evolution of the Salton Sea inferred from seismic reflection data. Nature Geoscience, 2(8), (2009), pp.581-584. https://doi.org/10.1038/ngeo590

California Geologic Energy Management (CalGEM) Division: Well Finder, www.conservation.ca.gov/calgem/Pages/WellFinder.aspx, Accessed 1 Jan. 2024.

Elders, W.A., Rex, R.W., Robinson, P.T., Biehler, S. and Meidav, T.: Crustal Spreading in Southern California: The Imperial Valley and the Gulf of California formed by the rifting apart of a continental plate, Science, 178(4056), (1972), pp.15-24. https://doi.org/10.1126/science.178.4056.15

Esri: World Elevation Hillshade, 1:1,000,000 scale, (2024).

Fuis, G.S., and Kohler, W.M.: Crustal structure and tectonics of the Imperial Valley region, California, in Rigsby, C.A., ed., The Imperial Basin—Tectonics, sedimentation and thermal aspects: Los Angeles, Pacific Section, Society of Economic Paleontologists and Mineralogist, (1984), p. 1-13.

Glen, J.M.G., and Earney, T.E.: New High Resolution Airborne Geophysical Surveys In Nevada And California For Geothermal And Mineral Resource Studies, GRC Transactions, (2023), Vol. 47, 25p.

Glen, J.M.G., and Earney, T.E.: GeoFlight: Airborne magnetic and radiometric surveys of the Salton Trough, Southern California: U.S. Geological Survey data release, (2024). https://doi.org/10.5066/P14C7WNM

Han, L., Hole, J.A., Stock, J.M., Fuis, G.S., Williams, C.F., Delph, J.R., Davenport, K.K. and Livers, A.J.: Seismic imaging of the metamorphism of young sediment into new crystalline crust in the actively rifting Imperial Valley, California, Geochemistry, Geophysics, Geosystems, 17(11), (2016), pp.4566-4584. https://doi.org/10.1002/2016GC006610

Hildenbrand, T., Briesacher, A., Flanagan, G., Hinze, W., Hittleman, A., Keller, G., Kucks, R., Plouff, D., Roest, W., Seeley, J., Smith, D., and Webring, M.: Rationale and Operational Plan to Upgrade the U.S. Gravity Database, U.S. Geological Survey Open File Report, 02-463, (2002). https://doi.org/10.3133/ofr02463

Jachens, R.C. and Moring, B.C.: Maps of the thickness of Cenozoic deposits and the isostatic residual gravity over basement for Nevada (No. 90-404), US Dept. of the Interior, Geological Survey, (1990). https://doi.org/10.3133/ofr90404

Jachens, R.C., Moring, B.C., Schruben, P.G. and Singer, D.A.: Thickness of Cenozoic deposits and the isostatic residual gravity over basement. An analysis of Nevada's metal-bearing mineral resources: Nevada Bureau of Mines and Geology Open-File Report, (1996), pp.96-2.

Jennings, C.W., with modifications by Gutierrez, C., Bryant, W., Saucedo, G., and Wills, C.: Geologic map of California: California Geological Survey, Geologic Data Map No. 2, scale 1:750,000, (2010).

Lachenbruch, A.H., Sass, J.H. and Galanis Jr, S.P.: Heat flow in southernmost California and the origin of the Salton Trough. Journal of Geophysical Research: Solid Earth, 90(B8), (1985), pp.6709-6736. https://doi.org/10.1029/JB090iB08p06709

McKibben, M.A., Andes, J.P. and Williams, A.E.: Active ore formation at a brine interface in metamorphosed deltaic lacustrine sediments; the Salton Sea geothermal system, California, Economic Geology, 83(3), (1988), pp.511-523. https://doi.org/10.2113/gsecongeo.83.3.511

McKibben, M.A., Williams, A.E., Elders, W.A., and Eldridge, C.S.: Saline brines and Metallogenesis in a Modern Sediment-filled Rift: the Salton Sea Geothermal system, California, U.S.A., Applied Geochemistry, 2, (1987), 563-578. https://doi.org/10.1016/0883-2927(87)90009-6

National Renewable Energy Laboratory: U.S. Operating Geothermal Power Plants, (2014). https://www.nrel.gov/gis/geothermal

Nichols, E.: Geothermal Exploration Under the Salton Sea Using Marine Magnetotellurics, California Energy Commission, PIER Renewable Energy Technologies Program, CEC-500-2009-005, (2009).

Patrick Muffler, L.J. and White, D.E.: Active Metamorphism of Upper Cenozoic Sediments in the Salton Sea Geothermal Field and the Salton Trough, southeastern California, Geological Society of America Bulletin, 80(2), (1969), pp.157-182. https://doi.org/10.1130/0016-7606(1969)80[157:AMOUCS]2.0.CO;2

Persaud, P., Ma, Y., Stock, J.M., Hole, J.A., Fuis, G.S. and Han, L.: Fault zone characteristics and basin complexity in the southern Salton Trough, California. Geology, 44(9), (2016), pp.747-750. https://doi.org/10.1130/G38033.1

Saltus, R.W. and Jachens, R.C.: Gravity and basin-depth maps of the Basin and Range Province, western United States (No. 1012). (1995). https://doi.org/10.3133/gp1012

Schmitt, A.K. and Hulen, J.B.: Buried rhyolites within the active, high-temperature Salton Sea geothermal system, Journal of Volcanology and Geothermal Research, 178(4), (2008), pp.708-718. https://doi.org/10.1016/j.jvolgeores.2008.09.001

Tokmakoff, L., Share, P.E., Naif, S., Miller, A., Peacock, J.R., Constable, S., Ghalati, F.H.: Crustal Electrical Resistivity of Active Tectonic Structures in the Salton Trough: Insights from the MIST Project, AGU Fall Meeting Abstracts, (2024).

U.S. Geological Survey: Quaternary Fault and Fold Database for the Nation, U.S. Geological Survey data release, (2020). https://doi.org/10.5066/P9BCVRCK